PNAS Nexus, 2024, 3, 1–12
https://doi.org/10.1093/pnasnexus/pgae096
Advance access publication 1 March 2024
Research Report

A small molecule MST1/2 inhibitor accelerates murine liver regeneration with improved survival in models of steatohepatitis

Ryan Watkins[a], Ana Gamo[b,1], Seung Hyuk Choi[b,1], Manoj Kumar[b,1], EeeLN Buckarma[a], Chantal McCabe[c], Jennifer Tomlinson[a], David Pereya[d], Blaz Lupse[e], Shirin Geravandi[e], Nathan W. Werneburg[f], Chen Wang[c], Patrick Starlinger[a,g], Siying Zhu[b], Sijia Li[b], Shan Yu[b], Murali Surakattula[b], Tyler Baguley[b], Amin Ardestani[e,h], Kathrin Maedler[e], Jason Roland[b], Van Nguyen-Tran[b], Sean Joseph[b], Mike Petrassi[b], Nikki Rogers[b], Gregory Gores[f], Arnab Chatterjee[b,2*], Matthew Tremblay[b,2*], Weijun Shen[b,2*] and Rory Smoot[a,i,2*]

[a]Department of Surgery, Mayo Clinic, Rochester, MN 55905, USA
[b]Calibr at Scripps Research, The Scripps Research Institute, La Jolla, CA 92037, USA
[c]Division of Biomedical Statistics and Informatics, Mayo Clinic, Rochester, MN 55905, USA
[d]Department of Surgery, Medical University of Vienna, General Hospital, Vienna 1090, Austria
[e]Centre for Biomolecular Interactions Bremen, University of Bremen, 28359 Bremen, Germany
[f]Division of Gastroenterology and Hepatology, Mayo Clinic, Rochester, MN 55905, USA
[g]Center of Physiology and Pharmacology, Medical University of Vienna, Vienna 1090, Austria
[h]Biomedical Institute for Multimorbidity (BIM), Centre for Biomedicine, Hull York Medical School, University of Hull, Hull YO10 5DD, UK
[i]Department of Biochemistry and Molecular Biology, Mayo Clinic, Rochester, MN 55905, USA
*To whom correspondence should be addressed: Email: smoot.rory@mayo.edu (R.S.); Email: wshen@szbl.ac.cn (W.S.); Email: matt@blackbirds.org (M.T.); Email: acharterjee@scripps.edu (A.C.)
[1]A.G., S.H.C., and M.K. contributed equally to this work.
[2]A.C., M.T., W.S., and R.S. contributed equally to this work.
Edited By: David Brenner

Abstract

Dysfunctional liver regeneration following surgical resection remains a major cause of postoperative mortality and has no therapeutic options. Without targeted therapies, the current treatment paradigm relies on supportive therapy until homeostasis can be achieved. Pharmacologic acceleration of regeneration represents an alternative therapeutic avenue. Therefore, we aimed to generate a small molecule inhibitor that could accelerate liver regeneration with an emphasis on diseased models, which represent a significant portion of patients who require surgical resection and are often not studied. Utilizing a clinically approved small molecule inhibitor as a parent compound, standard medicinal chemistry approaches were utilized to generate a small molecule inhibitor targeting serine/threonine kinase 4/3 (MST1/2) with reduced off-target effects. This compound, mCLC846, was then applied to preclinical models of murine partial hepatectomy, which included models of diet-induced metabolic dysfunction-associated steatohepatitis (MASH). mCLC846 demonstrated on target inhibition of MST1/2 and reduced epidermal growth factor receptor inhibition. The inhibitory effects resulted in restored pancreatic beta-cell function and survival under diabetogenic conditions. Liver-specific cell-line exposure resulted in Yes-associated protein activation. Oral delivery of mCLC846 perioperatively resulted in accelerated murine liver regeneration and improved survival in diet-induced MASH models. Bulk transcriptional analysis of regenerating liver remnants suggested that mCLC846 enhanced the normal regenerative pathways and induced them following liver resection. Overall, pharmacological acceleration of liver regeneration with mCLC846 was feasible, had an acceptable therapeutic index, and provided a survival benefit in models of diet-induced MASH.

Keywords: Hippo, medicinal chemistry, MASH, YAP, TAZ

Significance Statement

Liver regeneration relies on a highly regulated response to maintain homeostasis after surgical resection. Disruption of this process, which can be seen in metabolic dysfunction-associated steatotic liver disease (MASLD), can result in morbidity and mortality. Currently, no pharmacologic agents are approved for use to augment liver regeneration or prevent liver dysfunction after surgical resection. Our work optimized a small molecule inhibitor, mCLC846. In murine models of hepatectomy, mCLC846 resulted in accelerated liver regeneration and a survival advantage in mice with a severe form of MASLD. Our work demonstrates that small molecule inhibitors could be used to accelerate liver regeneration and potentially prevent liver dysfunction following surgical resection in healthy and diseased states.

Competing Interest: A provisional patent application of the MST1/2 inhibitors has been filed, and A.C., W.S., Matt S. Tremblay, Nikki Alvarez, H. Michael Petrassi, and Ana M. Gamo from Calibr at Scripps Research are co-inventors of the provisional filing.
Received: October 7, 2023. **Accepted:** February 20, 2024

Introduction

Liver regeneration is a complex and tightly regulated process, of which our understanding continues to rapidly evolve. Yes-associated protein (YAP), a transcriptional coactivator, has consistently been shown to play a role in the process of liver regeneration (1–3). We, and others, have shown that activating YAP can augment or accelerate liver regeneration (4–6). The Hippo pathway is a series of serine/threonine kinases that phosphorylate and inhibit YAP, and its paralog TAZ (7). Thus, inhibition of this pathway results in YAP activation. Serine/threonine kinase 4/3 (MST1/2) is a key component of the Hippo signaling cascade, which lies upstream of the Mps one Binder (MOB1)-LATS (1/2) kinase relay module and plays a key role in liver regeneration termination, where it is normally upregulated transiently posthepatectomy (6). MST1/2 inhibition or genetic ablation in the liver increases YAP activity, augments liver regeneration, and increases organ size (5, 6). This effect is so potent that extended loss of MST1/2 signaling through genetic deletion can result in hepatocarcinogenesis and thus must be tightly regulated (8).

Posthepatectomy liver failure (PHLF) represents a spectrum of disease ranging from limited hepatic insufficiency to acute fulminant hepatic failure following liver resection (9). PHLF represents the number one cause of postoperative mortality, and there are no effective treatment options (10). There are multiple risk factors for PHLF, but underlying liver disease, such as steatotic liver disease, greatly increases the risk of PHLF (11). Metabolic dysfunction-associated steatotic liver disease (MASLD) represents a clinical spectrum of disease from simple steatosis to metabolic dysfunction-associated steatohepatitis (MASH) (12). MASLD, as a risk factor for liver injury and PHLF, is particularly important, as the prevalence of MASLD is estimated to be 30% in the United States with escalating prevalence (13). Consistent with clinical outcomes in patients with MASH, preclinical models of MASH also demonstrate significant risk for mortality following partial hepatectomy (10). The ability to augment or accelerate liver regeneration pharmacologically, in patients with or without MASH, may provide an avenue for prevention or treatment of PHLF. Additionally, chronic liver disease progressed to end-stage liver disease can be treated with orthotopic liver transplantation. The availability of suitable organs for transplantation continues to be limited and expanding donor criteria to include steatotic livers continues to be investigated (14). Pharmacologic enhancement of liver regeneration when utilizing suboptimal donors could be of utility.

Neratinib is a clinically approved, epidermal growth factor receptor (EGFR)/EGFR2 small molecule inhibitor used in the treatment of breast cancer (15). Previously, neratinib was identified to have high MST1 inhibitory activity in a high-throughput MST1 inhibition screen (16, 17). Given these properties, structure–activity relationship (SAR) approaches were utilized to maintain the MST1/2 activity while reducing EGFR inhibitory effects. In this study, we describe the medicinal chemistry approaches utilized to generate mCLC846, an orally bioavailable MST1/2 inhibitor utilizing a neratinib backbone. We examined the effects of mCLC846 on the regenerative capacity of the liver in murine models of partial hepatectomy, including in clinically relevant models of hepatic steatosis. These studies suggest that mCLC846 inhibits MST1/2, thereby inducing YAP-dependent proregenerative signaling, augmenting liver regeneration, and improving survival in a murine MASH model following partial hepatectomy.

Materials and methods

In vitro studies

Normal human cholangiocytes (NHCs) were maintained in culture, as previously described, at 37 °C and 5% CO_2 (18). Experiments with NHC were performed in Dulbecco's Modified Eagle Medium (DMEM) with 10% fetal bovine serum (FBS) with cells at 60–80% confluency unless otherwise specified. Hu1545 cells, a hepatocyte-derived cell line, were kindly provided by Keith Robertson (Mayo Clinic, Rochester, MN, USA) and were cultured, as previously described, in DMEM with 10% FBS (19). HepG2 cells were obtained from ATCC and maintained as recommended.

Cell proliferation

Hu1545, NHC, and HepG2 cells were plated in 96-well plate in equal number. Cells were then exposed to mCLC846 or vehicle (dimethylsulfoxide, DMSO). Seventy-two hours following exposure relative cell viability was determined with the CellTiter-Glo Luminescent Cell Viability Assay (Promega, Madison, WI, USA), according to the manufacturer's recommendations.

The clonal rat β-cell line INS1E was kindly provided by Dr Claes Wollheim, Geneva, and Lund University. Human islets were isolated from four pancreases of nondiabetic organ donors at PRODO Labs and at Lille University and cultured on Biocoat Collagen I–coated dishes (#356400, Corning, ME, USA), as described earlier (20).

INS1E and human islets were cultured in complete RPMI-1640 at 11.1 mM or CMRL-1066 medium at 5.5 mM glucose, respectively, as previously described (21). Cells were cultured in variable conditions, which include: 22.2 mM glucose, 0.5 mM palmitic acid (PA), dissolved as previously described (22), 1 mM thapsigargin (TG), 100 µM hydrogen peroxide (H_2O_2; all Sigma) with or without mCLC846.

INS1E cells were treated with compounds in dose-dependent manner in 384 well microplates (Corning, NY, USA) at 10^4 cells/well in 25 µL of complete grow medium. After 24 h of compound treatment, 5 µL of Celltiter-Glo reagent (Promega) was added to each well. Assay plates were shaken vigorously for 1 min at room temperature to achieve complete cell lysis. Luminescence intensity was detected on an Envision plate reader (Perkin Elmer).

MST1/MST2 protein expression, purification, crystallization, and data collection

The kinase domain of MST1-containing amino acid residues (25–301) and the kinase domain of MST2-containing amino acid residues (24–300) were cloned into the pET-15b vector and expressed as a His-tag fusion protein in the *Escherichia coli* BL21 (DE3) cells. Cell culture was carried out in terrific broth (TB) media at 18 °C. The fusion protein was purified by a nickel affinity column and further purified by anion exchange chromatography and Superdex 75 16/60 column. The nearly pure protein samples were concentrated to 10 mg/mL in 25 mM 4-(2-hydroxyethyl)-1-piperazineethanesulfonic acid (HEPES) (pH 7.5), 150 mM NaCl, 5% glycerol, 1 mM Tris (2-chloroethyl) phosphate (TCEP), 2 mM $MgCl_2$.

Animals

C57BL/J6 mice were obtained from JAX Laboratory, USA. Mice were maintained under a 12-h light dark cycle (6 AM to 6 PM) and fed ad libitum. Interventions were only performed during

Table 1. Pharmacokinetic properties of neratinib and mCLC846 in mice.

	Neratinib PO (20 mg/kg)	mCLC846 IV (5 mg/kg)	mCLC846 PO (20 mg/kg)
C_{max} (ng/mL)	342 ± 152	1,047 ± 80	384 ± 128
AUC $_{0\text{-last}}$ (ng h/mL)	3,115 ± 1,358	2,585 ± 85	3,675 ± 854
T_{max} (h)	4.0 ± 3.0	0	1.7 ± 1.1
$T_{1/2}$ (h)	—	8.0 ± 1.6	10.3 ± 2.5
Mean residence time $(MRT)_{0\text{-last}}$ (h)	5.4 ± 1.3	4.0 ± 0.7	8.9 ± 0.3
F%	ND	ND	35

Table 2. Pharmacokintetic profile of mCLC846 in dogs and rats.

	Rat PO PK HCl salt (mg/kg)			Dog PO PK HCl salt (mg/kg)
	30	100	300	5
C_{max} (ng/mL)	256 ± 6.7	396 ± 118	8,005 ± 4,239	210 ± 134
$AUC_{0\text{-last}}$ (ng h/mL)	1,303 ± 124	2,724 ± 771	69,942 ± 22,400	1,451 ± 617
T_{max} (h)	3 ± 0	3 ± 0	3 ± 0	0.67 ± 0.29
$T_{1/2}$ (h)	6.7 ± 1.4	8.0 ± 1.6	10.2 ± 2.4	6.70 ± 0.75
Mean residence time $(MRT)_{0\text{-last}}$ (h)	6.74 ± 0.45	8.8 ± 0.9	11.8 ± 1.4	8.41 ± 0.89
F%	20	12	100	37

their light cycle and completed at the same time within their light cycle.

MASH model

Ten-week-old male C57BL/J6 were housed 5 mice per cage, and cages were randomized to a diet for 24 weeks: standard chow (Diet Pico Laboratory Rodent Diet) or high fat, fructose, and cholesterol (FFC) diet which included a high fat and cholesterol chow (AIN-76A Western Diet; 1810060; Test Diet) and drinking water supplemented with fructose (23.1 g/L, Sigma F2543) and glucose (18.9 g/L, Sigma 49158), as previously described (23).

Pharmacokinetic property determination in vivo

Pharmacokinetic properties of mCLC846 were assessed in CD1 female mice (Table 1), Sprague–Dawley male rats (Table 2), and male beagle dogs (Table 2). The compound was prepared in 0.5% methylcellulose:0.5% Tween-80 for oral (PO) administration and in saline for intravenous (IV) administration. Dosing volume (5 mL/kg) was used for both IV and PO routes in mice, rats, and dogs. Following oral administration in mice and dogs, compound concentrations were measured in plasma samples collected at 30 min, 1 h, 3 h, 8 h, and 24 h postcompound administration. Following oral administration in rats, plasma was collected at 15 min, 1 h, 3 h, 8 h, 24 h, 32 h, 48 h, and 72 h. All procedures and animal handling were performed according to standard operating procedures approved by the Institutional Animal Care and Use Committee (IACUC) at each institution.

In vivo therapeutics

For the murine partial hepatectomy model, mice were treated 1 day preoperatively and then every 12 h postoperatively, until euthanasia unless otherwise noted. Mice received mCLC846 every 12 h via oral gavage dissolved in 0.5% methylcellulose + 0.5% Tween-80. Control mice received equal volumes of vehicle.

Partial hepatectomy model

Male age-matched mice were assigned to control or treatment. Surgical procedures were performed in small cohorts to ensure uniform timing in relation to the day:night cycle. Mice were anesthetized by vaporized isoflurane for an average operation time of 15 min. Seventy percent partial hepatectomy was conducted as previously described (24). Briefly, cholecystectomy followed by sequential ligation and excision of the left median, right median, and left lateral lobes was performed. Hemostasis was achieved. The abdomen was then closed in 2 layers with running 4-0 Vicryl. The resected tissue was collected for further molecular analysis as baseline. Liver regeneration was assessed at 40 and 72 h posthepatectomy. All excised tissue was either frozen and stored at −80 C or fixed in 10% (v/v) buffered formalin overnight at room temperature.

YAP/TAZ hepatocyte deletion in vivo

Yap/Taz double floxed mice ($Yap^{fl/fl}/Taz^{fl/fl}$) were obtained from Jackson Laboratory (Strain #030532). Eight-week-old $Yap^{fl/fl}/Taz^{fl/fl}$ mice were administered 1×10^{11} AAV8 particles expressing AAV.TBG.PI.Cre.rBG, a gift from James M. Wilson (Addgene viral prep # 100787-AAV8) as previously described, intravenously by tail vein injection (25). Four weeks following administration, mice underwent 70% partial hepatectomy as described above.

Plasma analysis posthepatectomy

Blood was collected via inferior vena cava puncture and placed in a lithium heparin tube. Plasma was separated from the blood by centrifugation at $2{,}000 \times g$ for 15 min at 4 °C and transferred to new tubes. Plasma was aliquoted and stored at −80 °C. Plasma was analyzed with Vetscan VS2 chemistry analyzer (Zoetis). Plasma glucose was analyzed using a Bayer Contour Next EZ glucometer (Bayer, USA).

RNA sequencing

RNA was isolated from mouse livers using Qiagen RNeasy kit with on column DNase digestion per the manufacturer protocol. The raw RNA sequencing paired-end reads for the samples were processed through the Mayo RNA-Seq bioinformatics pipeline, MAP-RSeq version 3.1.4 (26). Briefly, MAP-RSeq employs the very fast, accurate, and splice-aware aligner, STAR (27), to align reads to the reference human genome build hg38. The aligned reads were then processed through a variety of modules in a parallel fashion. Gene and exon expression quantification were performed using the Subread (28) package to obtain both raw and normalized reads (reads per kilobase per million mapped reads). Finally, comprehensive analyses were run on the aligned reads to assess the quality of the sequenced libraries. The data presented in this publication have been deposited to NCBI's Gene Expression Omnibus (GEO) and are accessible through GEO Series accession number GSE231391. Using the raw gene counts report from MAP-RSeq, genes differentially expressed between the groups were assessed using the bioinformatics package edgeR 2.6.2 (29). Genes found different between the groups were reported along with their magnitude of change (Log_2 scale) and their level of significance (false

discovery rate, FDR < 5%). Canonical pathway analysis was performed using the ingenuity pathway analysis (IPA) software (Ingenuity Systems). Biological functions and disease information within the IPA software were used to investigate the canonical pathways of interest. The ShinyGO application was used to evaluate the core regeneration gene sets, as previously described (30). Pathways were considered significant using FDR<5%.

qRT-PCR

Total RNA was isolated from cultured cells or mouse liver samples using TRIzol followed by isopropanol precipitation. Reverse transcription was performed with Moloney murine leukemia virus reverse transcriptase and random primers (Life Technologies). Real-time PCR (Light Cycler 480 II, Roche Diagnostics) was performed with Sybr Green (Roche Diagnostics) with primer sequences listed in Table S1. Relative expression of target genes was calculated using the ΔΔCt method with target gene normalization to the geometric mean of 18S rRNA expression.

Western blot

Proteins were isolated from mouse livers or cell lysates by mechanical disruption in cell lysis buffer (Cell Signaling Technology) with protease inhibitors (Roche), phosphatase inhibitors (Roche), and 1 mM phenylmethylsulfonyl fluoride (PMSF). Cellular debris was removed by centrifugation, 12,000 × *g* 15 min at 4 °C. Protein concentrations were determined with bovine serum albumin (BSA) protein assay (Fisher). Proteins were resolved by sodium dodecyl sulfate–polyacrylamide gel electrophoresis (SDS–PAGE) on Tris-Glycine gels (Invitrogen) followed by transfer to 0.2 µm nitrocellulose or polyvinylidene fluoride (PVDF). Membranes were blocked with 5% BSA in TBS-Tween-20 (0.1% v/v) and then stained overnight at 4 °C. Primary antibodies are listed in Table S2. Secondary horseraddish peroxidase (HRP) antibodies were applied for 1 h at room temperature, and then blots were visualized with ECL or ECL prime (GE Healthcare Life Sciences) chemiluminescence. Membranes were stripped, blocked, and reblotted as needed.

5-Bromo-2′-deoxyuridine labeling

Two hours prior to euthanasia, mice were administered 5′-bromo-2′-deoxyuridine (100 mg/kg; Sigma) i.p. Formalin fixed paraffin embedded (FFPE) liver sections were incubated with primary antibody at 4 °C overnight. Secondary antibody was applied for 1.5 h at room temperature, and nuclei were counterstained with DAPI. Ten high-powered fields (400×) were visualized, and 5-bromo-2′-deoxyuridine (BrdU)-positive hepatocytes were counted on an immunofluorescence microscope (Invitrogen EVOS M5000).

Immunohistochemistry

Paraffin sections were cut at a thickness of 5 µm. Tissues that were stained for histological analysis with hematoxylin and eosin (H&E) or primary antibodies are listed in Table S2. For quantification of BrdU-positive hepatocytes, 10 high-power fields (200×) were visualized per sample and manually counted. β-Cell apoptosis was analyzed in bouin-fixed, agarose-pelleted, paraffin-embedded human islets by the terminal deoxynucleotidyl transferase-mediated dUTP nick-end labeling technique, according to the manufacturer's instructions (In Situ Cell Death Detection Kit, Roche) and double stained for insulin and analyzed using a Nikon MEA53200 (Nikon GmbH, Dusseldorf, Germany) microscope, and images were acquired using NIS-Elements software (Nikon) as described before (17).

Statistical analysis

Statistical analysis was performed with Prism version 9 (GraphPad Software) software or SPSS (IBM SPSS Statistics). Comparison of two groups for in vitro and in vivo studies was performed using Mann–Whitney *U* test. Comparison of three or more groups was performed using Kruskal–Wallis test. Survival analysis was performed using Log-Rank (Mantel Cox) test in SPSS. *P*-values <0.05 were considered statistically significant. Statistical significance is represented in figures as follows: ns $P > 0.05$, $^{*}P < 0.05$, $^{**}P < 0.01$, and $^{***}P < 0.001$.

Study approval

All animal experiments performed at the Mayo Clinic were approved by the Mayo Clinic IACUC. Human islet experiments were performed in the islet biology laboratory, University of Bremen. Ethical approval for the use of human islets had been granted by the Ethics Committee of the University of Bremen. The study complied with all relevant ethical regulations for work with human cells for research purposes. Organ donors are not identifiable and anonymous, and the approved experiments using human islet cells for research are covered by the NIH Exemption 4 (Regulation PHS 398).

Results

Medicinal chemistry optimization generates an MST1/2 inhibitor

Inhibition of MST1/2 has proven beneficial in multiple disease processes, including diabetes, inflammatory bowel disease, liver injury, and myocardial injury (5, 16, 31). Neratinib is an FDA-approved, antineoplastic compound that inhibits receptor tyrosine kinases like EGFR. In addition to its receptor tyrosine activity, it was also identified as a potent MST1/2 inhibitor (16, 17). Given the known benefits of MST1/2 inhibition in modulating YAP activity, neratinib was identified as a potential parent compound for the development of a regenerative therapeutic. Therefore, we initiated SAR medicinal chemistry approaches to generate compounds that had optimized MST1 inhibition with reduced potency against EGFR.

Neratinib is a covalent inhibitor of EGFR with subnanomolar potency ($IC_{50} = 0.72$ nM; Fig. 1A) with good absorption, distribution, metabolism, and excretion pharmacokinetic profile. Utilizing the neratinib backbone for optimization, the affinity for EGFR and MST1 was compared with the parent compound after each optimization process. Neratinib forms a covalent bond with Cys-773 on the ATP-binding site of EGFR, but importantly, this interaction is not critical for MST1 inhibition due to the lack of an equivalent cysteine residue. Thus, the electrophilic acrylamide, which functioned as a Michael acceptor in Neratinib, was replaced with 4-dimethylamino-butylamide in mBNB885. This adaptation resulted in 5-fold reduction in potency toward EGFR ($IC_{50} = 1.42$ nM) but preserved MST1 activity (Fig. S1A). Next, a focused SAR study was performed on the pyridine moiety and aniline ring of mBNB885. The pyridine ring has an important role for MST1 inhibition and a subtle change by the incorporation of a methyl group in position 6 resulted in mBOW183 with 6-fold increase in MST1 activity ($IC_{50} = 7.1$ nM; Fig. S1A). Moving the chlorosubstitution from the *para* to *ortho* position in relation to the aniline amine resulted in mCAR432 with a 3- to 4-fold

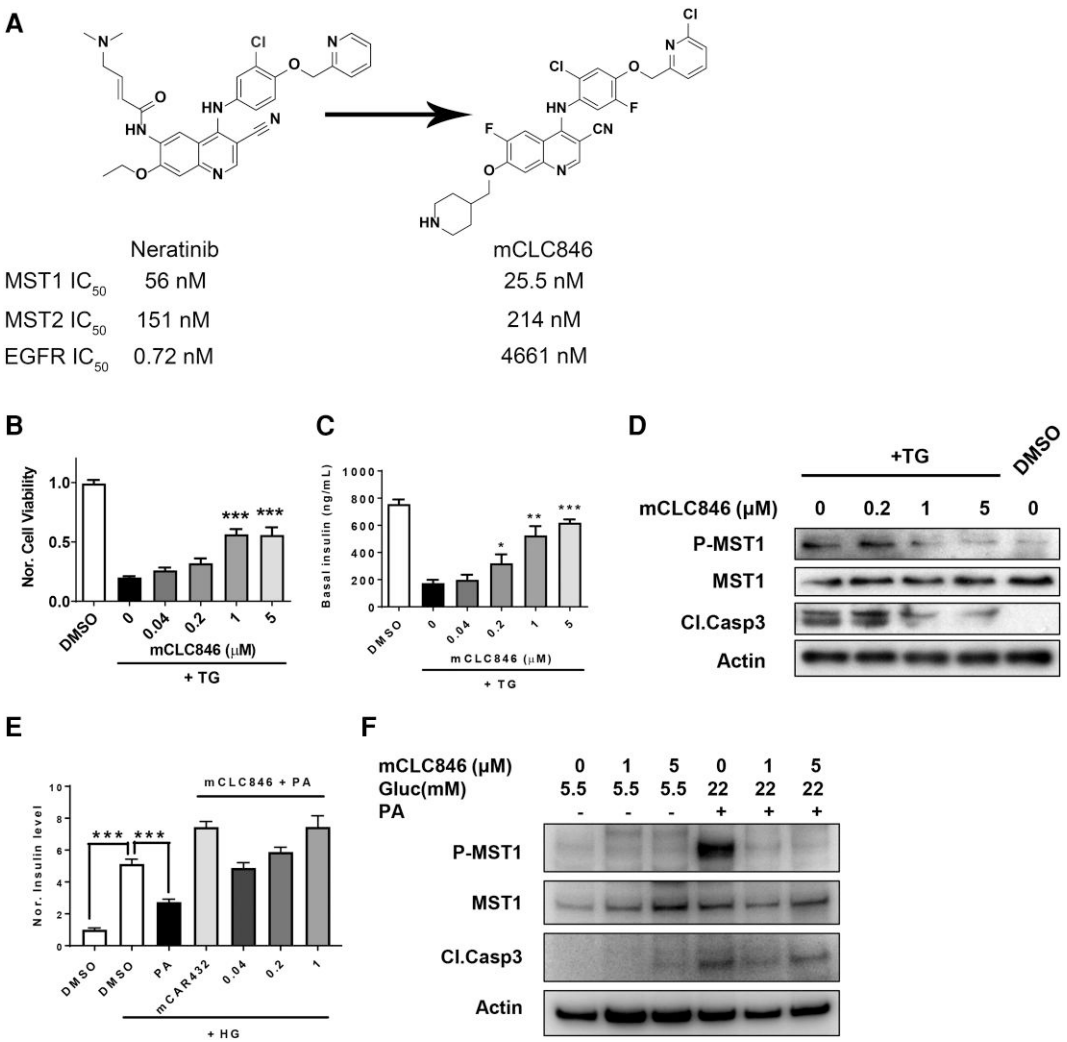

Fig. 1. mCLC846 inhibits MST1/2 and protects islet cells from toxic stimuli in vitro. A) Chemical structures of neratinib and mCLC846 with respective half maximal inhibitory concentrations (IC_{50}) for MST1, MST2, and EGFR. B) Normalized cell viability and C) insulin production of INS1E exposed to TG with or without mCLC846 ($n = 3$). D) Immunoblot of MST1 and cleaved caspase 3 (Cl.Casp3) from INS1E cell lysates following exposure to TG and/or mCLC846. E) Normalized insulin secretion from INS1E following exposure HG in the presence of PA, mCAR432, mCLC846 (μM), or mCLC846 and PA ($n = 3$). F) Human islet donor cell lysate immunoblot for MST1 and cleaved caspase 3 under conditions in E, representative sample from two donors.

improvement in MST1 inhibition ($IC_{50} = 9.8$ nM) and an approximately 500-fold reduction in EGFR inhibition ($IC_{50} = 379$ nM; Fig. S1A).

mCAR432 was further modified by the addition of a piperidine moiety to position 7, which contained a protonable amine bridge. mCED679 maintained MST1 inhibition ($IC_{50} = 25.5$ nM). We further explored the SAR of the pyridine moiety and the aniline ring on this new scaffold and identified mCLC846 (Fig. 1A) which maintained MST1 activity ($IC_{50} = 26.3$ nM), MST2 activity ($IC_{50} = 214$ nM), and reduced EGFR inhibition ($IC_{50} = 4{,}661$ nM). The reduced EGFR potency and maintained MST1/2 potency were satisfactory and elected to pursue further testing in vitro and in vivo. To obtain an unbiased assessment of kinase inhibition, mCLC846 was profiled against a panel of 50 kinases at Nanosyn (www.nanosyn.com). These results are displayed in Fig. S1B, which demonstrate activity to additional kinases. Overall, these results demonstrate the utility of SAR medicinal chemistry approaches and how they enabled the generation of a new MST1/2 inhibitor.

mCLC846 protects islet cells in diabetogenic conditions in vitro

MST1 is a key regulator in beta cells under diabetogenic conditions (21). We have previously shown that the MST1/2 inhibitory effects of neratinib were cytoprotective to pancreatic beta cells (16). As a mechanistic validation process, we evaluated the effects of mCLC846 on the pancreatic beta-cell line INS1E given the effects of MST1 inhibition have been well described previously. Cell viability and insulin production were measured in vitro in cells pretreated with mCLC846 at increasing doses prior to exposure with TG, a known ER stressor that induces beta-cell dysfunction and death. mCLC846 improved cell viability (Fig. 1B) and maintained basal insulin production (Fig. 1C) when compared with no treatment. To understand the potential mechanism of cytoprotection, activation of MST-1 and caspase 3 was interrogated by western blot. TG increased phosphorylation of MST-1, an activating mark, and increased cleaved caspase 3. Both MST1 activation and caspase 3 activation were reduced by pretreatment with mCLC846 (Fig. 1D). Additionally, mCLC846-treated INS1E cells

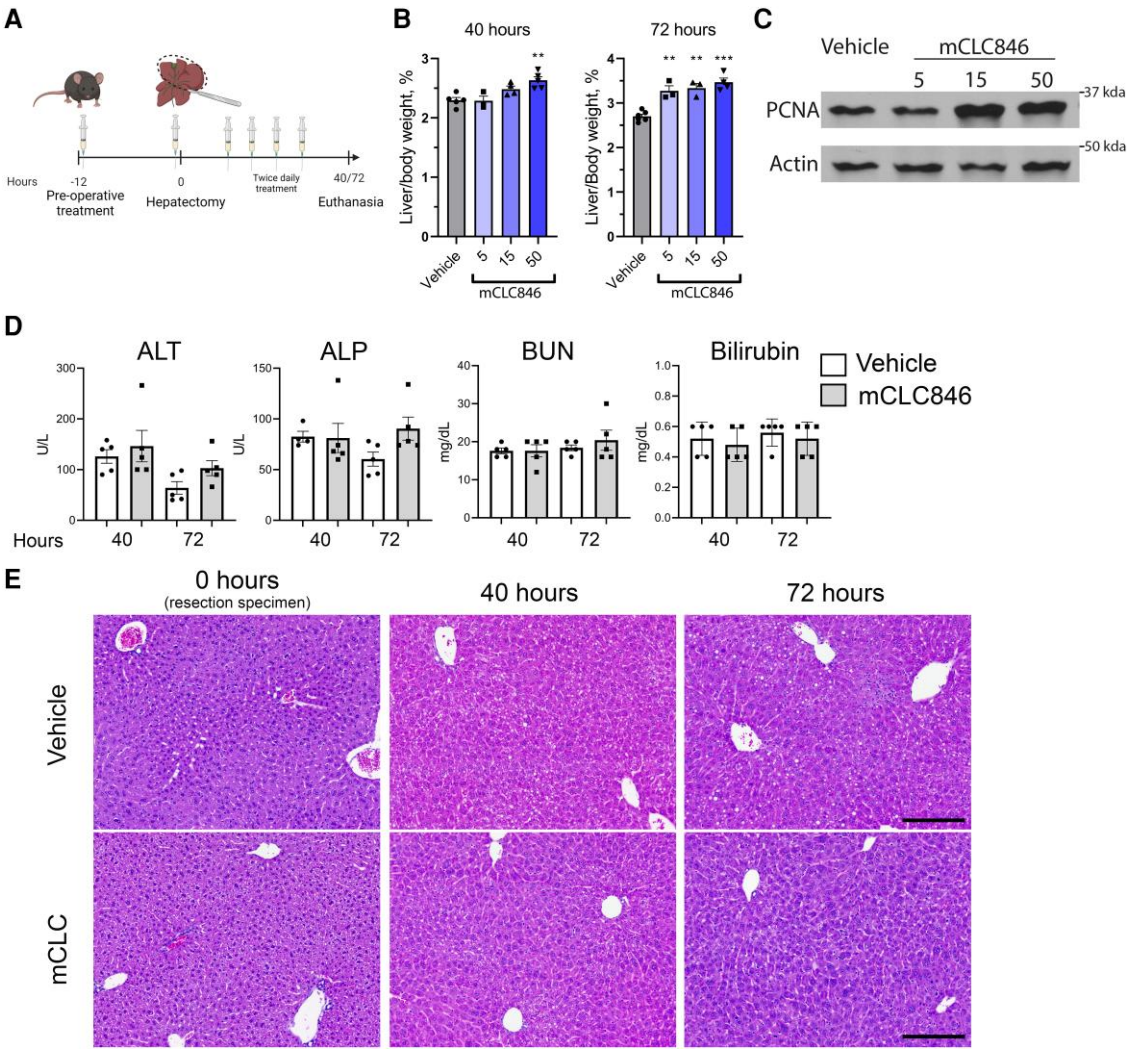

Fig. 2. mCLC846 accelerates murine liver regeneration following hepatectomy. A) Murine partial hepatectomy schema. B) Liver-to-body-weight ratio (%) following murine partial hepatectomy treated with vehicle or mCLC846 (mg/kg/dose) 40 and 72 h posthepatectomy ($n = 3$–6). C) Immunoblot for PCNA of liver lysates 40-h posthepatectomy treated with vehicle or mCLC846 (mg/kg/dose). D) Posthepatectomy plasma analysis of ALT, ALP, BUN, and total bilirubin in vehicle and mCLC846 (50 mg/kg/dose)-treated mice ($n = 5$). E) Representative H&E–stained liver resection and liver remnants treated with vehicle or mCLC846 (50 mg/kg/dose). Scale bar = 200 µm.

maintained their ability to secrete insulin in response to high glucose (HG) under the PA-induced cellular stress, glucolipotoxicity (Fig. 1E). Glucolipotoxicity-induced activation of MST-1 and increased cleaved caspase 3 levels were mitigated by pretreatment with mCLC846 in isolated human islets (Fig. 1F). The prosurvival effect of mCLCL846 was further evaluated microscopically in human islet utilizing mCAR432 (Fig. S1C).

These in vitro results mirrored our prior studies on the effects of MST1 inhibition in pancreatic beta cells. The data suggest that mCLC846 is cytoprotective through on target MST1 inhibition and reduction of caspase 3 activation in cytotoxic environments.

mCLC846 is orally bioavailable

mCLC846 pharmacokinetics were first evaluated in mice and compared with the parent compound neratinib. mCLC846 demonstrated comparable oral bioavailability with neratinib at 35% and good exposure (Table 1). Similar pharmacokinetics were observed in dogs treated with mCLC846 (Table 2). We further profiled mCLC846 in rats across a range of doses. We observed good exposure in rats, showing multiples of exposure and demonstrating a broad window. Additionally, there was under-proportional drug exposure from 30 to 100 mg/kg and over-proportional exposure at 300 mg/kg, suggesting saturation of a clearance mechanism (Table 2).

mCLC846 accelerates murine liver regeneration following partial hepatectomy

The activation of YAP has proven important in the context of liver regeneration. Activating YAP through genetic manipulation or pharmacological inhibition of the Hippo pathway has been utilized to accelerate liver regeneration (5). In a standard 70% murine partial hepatectomy model, mice were treated with variable doses of mCLC846 twice-daily beginning 12 h preoperatively (Fig. 2A). Liver regeneration was evaluated at 40 and 72 h posthepatectomy by examining liver-to-body-weight ratios. Forty hours posthepatectomy, liver-to-body-weight ratios were increased in mice treated with mCLC846 at 50 mg/kg/dose (Fig. 2B). Additionally, 72 h posthepatectomy liver-to-body-weight ratios were increased with mCLC846 at all doses tested (5, 15, and 50 mg/kg/dose;

Fig. 2B). Proliferative indices were evaluated 40 h posthepatectomy, a time point associated with peak proliferation (32), by proliferating cellular nuclear antigen (PCNA) immunoblot. PCNA was more abundant in murine liver lysates treated with mCLC846 in the 15 and 50 mg/kg/dose groups (Fig. 2C). Biochemical analysis did not identify any derangements in liver or kidney function tests, including alanine aminotransferase (ALT), alkaline phosphatase (ALP), blood urea nitrogen (BUN), and bilirubin (Fig. 2D). Histological analysis by H&E did not reveal any major changes in liver architecture pre- or posthepatectomy (Fig. 2E). These data indicate that perioperative mCLC846 accelerates liver regeneration posthepatectomy and is tolerable in the setting of partial hepatectomy.

mCLC846 activates YAP and TAZ, and is required for accelerated murine liver regeneration

MST1/2 is a kinase upstream of multiple Hippo pathway members, including MOB kinase activation 1A (MOB1A). Inhibition of MST1/2 is known to reduce MOB1A threonine phosphorylation, a marker of activity. The activity of MOB1A in conjunction with large tumor suppressor kinase 1/2 (LATS1/2) phosphorylates YAP at serine 127 (S127). This posttranslational modification marks YAP for cytosolic retention and degradation (33). Reduction of YAP serine phosphorylation permits nuclear translocation and transcriptional coactivation of cognate genes. Hu1545 cells, a human hepatocyte-derived cell line (19), were utilized to explore mCLC846 effects on YAP activation. First, MOB1A and YAP posttranslational modifications were observed with immunoblot following exposure to mCLC846 (3 μM). mCLC846-treated cells had reduced MOB1A phosphorylation, indicating target MST1/2 inhibition. Additionally, YAP^{S127} phosphorylation was reduced, suggesting increased YAP activity. H_2O_2 is known to activate the Hippo pathway through increased MST1/2 activation (20). Following exposure to H_2O_2, MOB1A phosphorylation increased, indicating increased MST1/2 activity. H_2O_2-induced MST1/2 activation was ablated, when Hu1545 cells were pretreated with mCLC846 (Fig. 3A).

YAP posttranslational changes were also examined over a range of mCLC846 doses (0.1–3 μM). Progressive decreases in serine phosphorylation were observed with increased mCLC846 dose (Fig. 3B). As previously discussed, changes in YAP^{S127} are known to be associated with subcellular redistribution of YAP and its paralog TAZ. Following, mCLC846 exposure YAP and TAZ subcellular locations were assessed, and mean fluorescence intensity was quantified by confocal microscopy. Hu1545 cells treated with mCLC846 demonstrated increased intranuclear levels of both YAP and TAZ, consistent with decreased Hippo pathway activity (Fig. 3C and D). To confirm that the posttranslational changes and YAP/TAZ nuclear relocation induced YAP/TAZ transcriptional coactivation, we further examined YAP/TAZ cognate gene expression. Using quantitative RT-PCR, *CTGF*, *CYR61*, and *NUAK2* were significantly increased in mCLC846-treated Hu1545 cells (Fig. 3E). Following exposure to mCLC846 in which cognate genes were elevated, mCLC846 was withdrawn, and cognate genes were reexamined 6 and 24 h later. *CTGF* and *NUAK2* remained elevated 6 h after mCLC846 withdrawal, and all cognate genes returned to baseline levels at 24 h (Fig. 3E). Hu1545 cells were exposed to mCLC846 for 72 h, and viable cell number was determined using an ATP luminescent assay. mCLC846-treated cells demonstrated increased cell viability which indicated that the small molecule inhibitor induced proliferation in vitro (Fig. 3F). These results indicate that mCLC846 inhibited MST1/2 in a human hepatocyte-derived cell line and resulted in transient YAP/TAZ activation, which was proproliferative.

To confirm the in vitro results, NHC, a transformed normal cholangiocyte cell line, was utilized to further define the effects of mCLC846 on YAP activity. Similar to observations in Hu1545, NHC cells exposed to mCLC846 demonstrated reduced serine phosphorylated YAP (Fig. S2A), increased expression of YAP/TAZ cognate gene expression (Fig. S2B), and increased cellular proliferation (Fig. S2C). Additionally, HepG2 cells, a cancerous cell line, were exposed to mCLC846 which induced a proliferative response (Fig. S2D).

Prior studies on MST1/2 inhibition or genetic ablation have shown that this alteration can induce liver carcinogenesis (8). Additionally, evidence suggests that disordered overactivity of YAP can promote fibrosis (34). To evaluate whether prolonged exposure to mCLC846 could lead to carcinogenesis or fibrosis, we administered mCLC846 (50 mg/kg/dose, twice daily) or vehicle (0.5% Tween-80/0.5% methylcellulose) for 4 weeks to mice. Following euthanasia, liver-to-body-weight ratio assessments were not different between treatment groups (Fig. S3A and B). Histological analysis with H&E and Sirius red stains did not identify any histological changes or fibrosis (Fig. S3C).

Resected livers from mice undergoing hepatectomy were interrogated to confirm mCLC846-inhibited MST1/2. Liver lysates were probed for phosphorylated MOB1, an immediate downstream target of MST1/2, where we observed a significant reduction in phosphorylated MOB1 indicating MST1/2 inhibition in vivo (Fig. 3G). We further investigated whether YAP/TAZ was a major determinant of accelerated liver regeneration observed with mCLC846 administration posthepatectomy. To do this, we genetically ablated *Yap* and *Taz* from hepatocytes in vivo by delivering hepatotropic Cre recombinase to $Yap^{fl/fl}/Taz^{fl/fl}$ mice as previously described (25) and outlined in Fig. S4A. YAP/TAZ deletion was confirmed by immunoblot of whole liver lysates from resection specimens (Fig. S4B). $Yap^{\Delta hep}/Taz^{\Delta hep}$ and $Yap^{fl/fl}/Taz^{fl/fl}$ mice, as a genetic background control, underwent partial hepatectomy with perioperative mCLC846 administration. Similar to wild-type mice, mCLC846 induced accelerated regeneration in $Yap^{fl/fl}/Taz^{fl/fl}$ mice but the proregenerative effects were lost in $Yap^{\Delta hep}/Taz^{\Delta hep}$ (Fig. 3G). These data indicate that mCLC846 mediates enhanced liver regeneration through YAP and TAZ.

mCLC846 induces a proregenerative transcriptional profile following hepatectomy

Due to YAP's importance in the downstream mediation of mCLC846-accelerated liver regeneration, we sought to further understand the transcriptional landscape in an unbiased fashion. Bulk RNA sequencing was performed on whole-liver lysates from vehicle- and mCLC846-treated mice 40 h posthepatectomy with resection specimens used as baseline measurements. Overall, the number of transcripts modified from baseline following hepatectomy in vehicle- and mCLC846-treated mice was similar, 1,224 vs. 1,463, respectively (Fig. 4A). The differentially expressed transcripts were compared between groups. Vehicle- and mCLC846-treated mice had 1,027 differentially expressed transcripts in common and 436 transcripts unique to mCLC846 treatment (Fig. 4A). These gene sets were characterized utilizing Qiagen IPA. The common gene set was enriched in pathways categorized as cell cycle regulation, cellular stress and injury, and metabolic pathways (complete list is given in the supplementary material). Activation scores (*Z*-score) were compared between the enriched pathways ($-1.3 < \text{Log2FC} > 1.3$, FDR < 0.05) from the

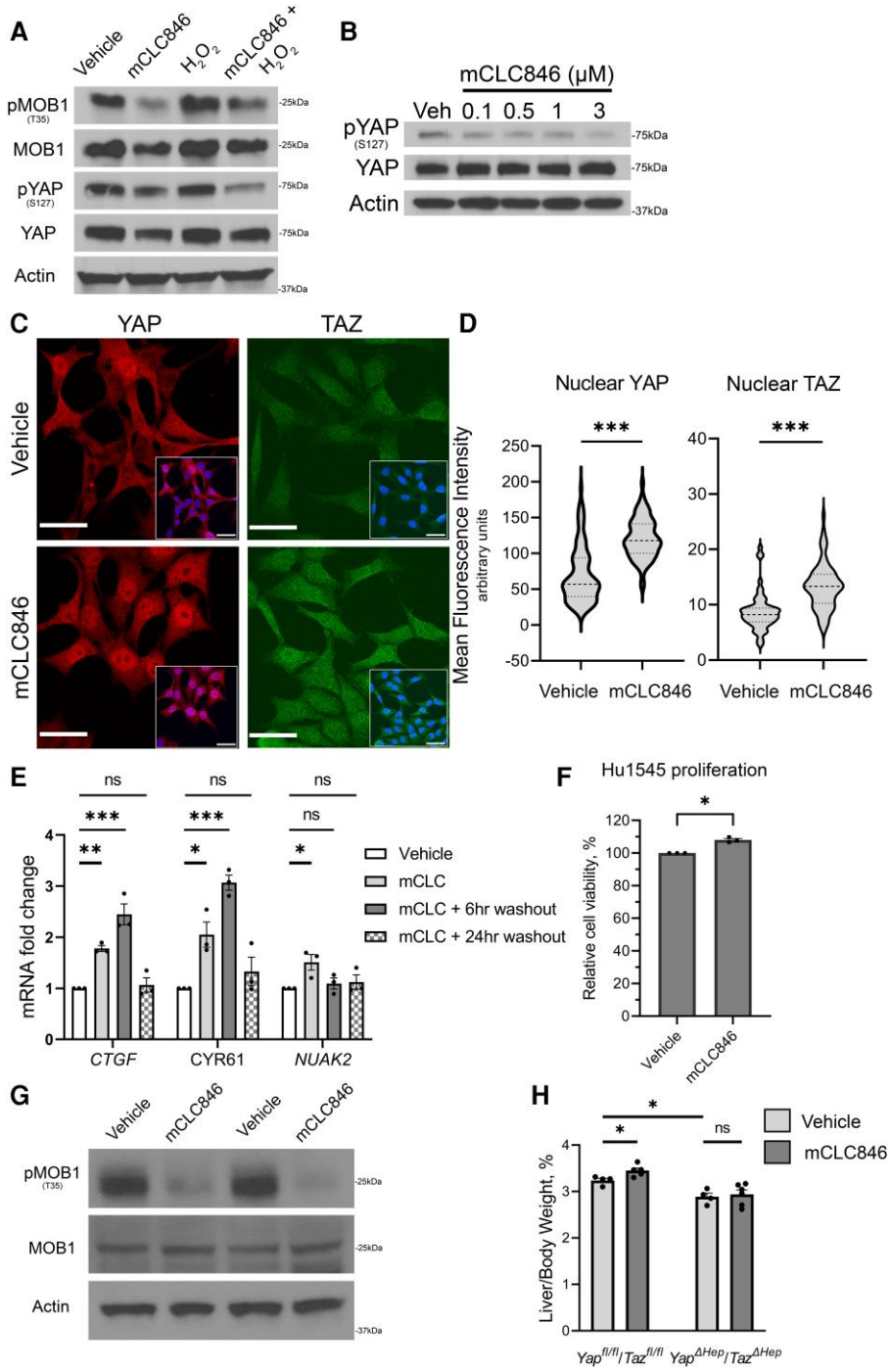

Fig. 3. mCLC846 transiently activates YAP in vitro in Hu1545 cells and is important for liver regeneration acceleration. A) Immunoblot detection of Mps one Binder (MOB1), Yes-associated protein (YAP), and their phosphorylated states in Hu1545 cell lysates following exposure of mCLC846 (3 μM) and/or H_2O_2. B) Immunoblot detection of YAP and its phosphorylated state following exposure to increasing concentrations of mCLC846 (μM). C) Representative immunofluorescence microscopy images of Hu1545 cells stained for YAP or TAZ following exposure to mCLC846 (3 μM). Image insets displaying DAPI overlay. Scale bar = 50 μm. D) Mean fluorescence intensity of nuclear YAP or TAZ in Hu1545 cells. Dashed line = median and dotted lines = interquartile range. E) Hu1545 transcript quantification by real-time-PCR following exposure to mCLC846 (3 μM), mCLC846 exposure 6 h, and 24 h after washout of mCLC846, normalized to vehicle expression ($n = 3$). F) Relative cell viability of Hu1545 cells following exposure to vehicle or mCLC846 (300 nM) for 72 h ($n = 3$). G) Murine resection liver specimen lysates pretreated with vehicle or mCLC846 phosphorylated MOB1 immunoblot with loading controls. Each lane represents a representative biological replicate ($n = 2$). H) Liver-to-body-weight ratio (%) in control $YAP^{fl/fl}/TAZ^{fl/fl}$ and mice with YAP/TAZ genetically ablated in hepatocytes, $YAP^{\Delta hep}/TAZ^{\Delta hep}$ treated with vehicle or mCLC846 (50 mg/kg/dose; $n = 4$–6).

transcripts unique to vehicle- or mCLC846-treated resected liver specimens. Pathways, in which an activation score was undefined or the Z-score change was between 1 and −1, were excluded from analysis. In mCLC846-treated mice, there was increased activation in inflammation related pathways which included IL-17 and MSP-RON signaling (Table S3). Pathways, in which the activation score was reduced in mCLC846-treated mice, were metabolic related (Table S3).

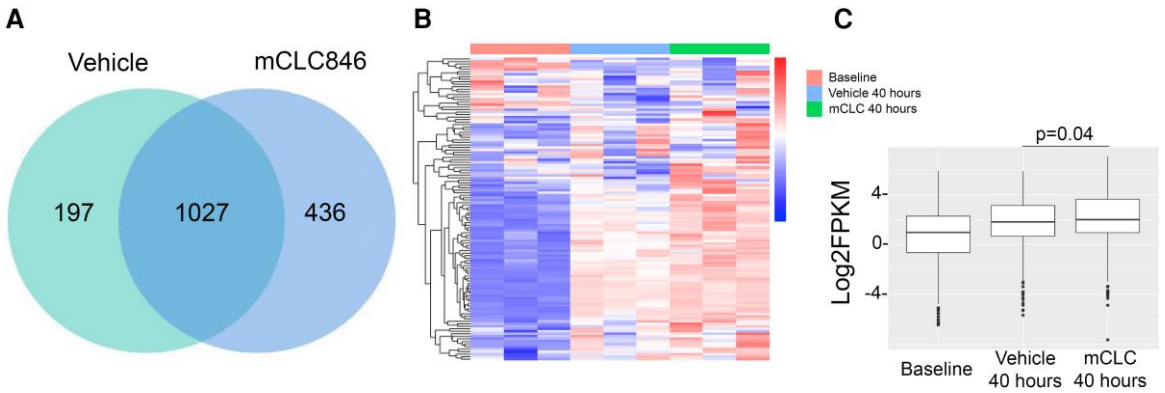

Fig. 4. mCLC846 induces accelerated liver regeneration through enhancement of normal regenerative pathways. A) Venn diagram of differentially expressed genes, 2 > Log_2-fold change <−2, 40 h posthepatectomy in vehicle- and mCLC846-treated mice. B and C) Heatmap and transcript expression quantification of cell cycle genes in murine livers at baseline and 40 h posthepatectomy in vehicle- and mCLC846-treated mice ($n = 3$).

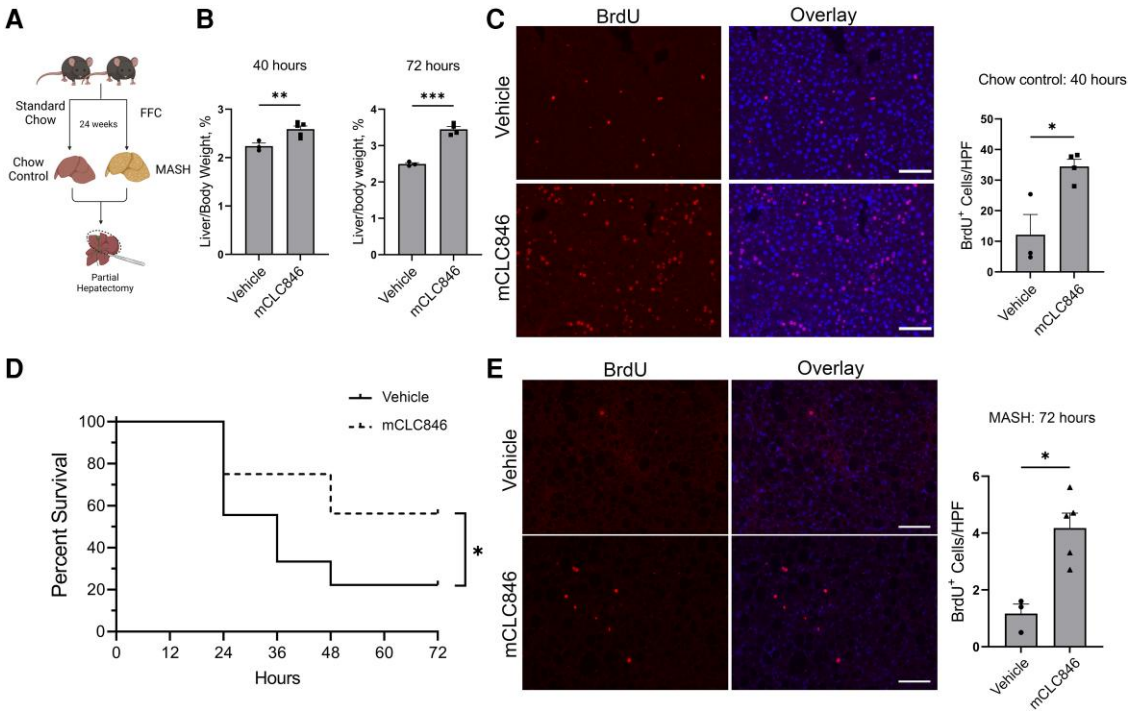

Fig. 5. mCLC846 prevents mortality following partial hepatectomy in diet-induced MASH models. A) Procedural schematic for MASH induction with a high FFC diet. B) Chow fed control mice liver-to-body-weight ratio (%) following hepatectomy with vehicle or mCLC846 (50 mg/kg/dose) treatment ($n = 3$–6). C) Representative immunofluorescence images and quantification of BrdU incorporation in murine liver sections 40 h posthepatectomy ($n = 3$–4). D) Murine MASH Kaplan–Meier survival curve posthepatectomy in vehicle- ($n = 18$) and mCLC846-treated animals ($n = 16$). Log-rank analysis. Vehicle $n = 18$ and mCLC846 $n = 16$. E) Representative immunofluorescence images and quantification of BrdU incorporation in MASH murine liver sections 72 h posthepatectomy ($n = 3$–5).

To confirm that mCLC846 induced a proproliferative enhancement of regeneration following partial hepatectomy, we compared the expression of transcripts to a standard cell cycle gene set (KEGG Cell Cycle, 04110). Cell cycle transcript expression at baseline and in the regenerating remnants of vehicle- and mCLC846-treated mice is graphically displayed in Fig. 4B. The hepatectomy stimulus alone induces increased expression of most cell cycle transcripts, as expected. Notably, mCLC846-treated mice had further induction of these cell cycle gene transcripts based on the Log2FPKM (Fig. 4C). These data indicate that mCLC846 administered perioperatively was proregenerative through enhanced induction of a core liver regeneration transcriptional profile.

mCLC846 improves posthepatectomy survival in murine diet-induced MASH

MASLD represents a spectrum of diseases that spans from simple steatosis to MASH. MASLD prevalence has increased over the past decade and represents a disease that increases the risk of liver insufficiency and PHLF following hepatectomy. The ability to prevent PHLF in patients with MASH represents the most critical need as the prevalence increases and carries the highest risk of mortality. Thus,

we sought to understand the effects of mCLC846 in a murine diet-induced MASH model following hepatectomy. Mice received either standard chow or a high FFC diet for 24 weeks as previously described (Fig. 5A) (23). MASH mice were characterized by increased weight gain and gross liver size (Fig. S5A and B). Microscopically, steatosis with ballooning hepatocytes and fibrosis was observed (Fig. S5C). Chow control mice were randomized to vehicle or mCLC846 treatment and underwent partial hepatectomy. Liver-to-body-weight ratio was increased at 40 and 72 h posthepatectomy in MASH mice compared with wild type (Fig. 5B). Proliferative response was assessed by BrdU incorporation. Liver sections at 40 h posthepatectomy demonstrated increased BrdU incorporation in mCLC846-treated mice (Fig. 5C). Partial hepatectomy in other murine MASH models has been shown to result in high postoperative mortality (4). Following partial hepatectomy, mice with diet-induced MASH had a 22.2% survival. Survival was significantly improved when MASH mice were treated with mCLC846 (56.25%) at 72 h posthepatectomy (Fig. 5D). Liver-to-body-weight ratio was not significantly increased in mCLC846-treated MASH mice (Fig. S5D). Despite the lack of liver-to-body-weight ratio augmentation, we again observed a significant increase in BrdU incorporation in mCLC846-treated mice (Fig. 5E). Hypoglycemia, following massive partial hepatectomy, has been identified as a cause of death postoperatively (35). Plasma glucose was measured 2 h following partial hepatectomy in MASH mice treated with either vehicle or mCLC846 and was not significantly different (Fig. S5E). These data indicate that administration of mCLCL846 in a murine model of MASH represents a feasible option to prevent liver failure and improve survival posthepatectomy. The exact mechanism for the improved survival is likely multifactorial and could be elucidated in further investigations.

Discussion

This study generated an MST1/2 inhibitor through medicinal chemistry approaches that induces proregenerative signaling and accelerates liver regeneration in models of murine partial hepatectomy. Specifically, the major findings of this study include: (i) mCLC846 is an orally bioavailable MST1/2 inhibitor with adequate tolerability, (ii) mCLC846 accelerated liver regeneration in models of murine partial hepatectomy by enhancing proregenerative transcription profiles, and (iii) mCLC846 improves survival in a diet-induced MASH partial hepatectomy model.

YAP activation via small molecule inhibitors has been associated with improved liver regeneration in mouse partial hepatectomy models (4, 5). In these models the inhibitors have targeted both classic components of the Hippo pathway, which acts as a negative regulator of YAP activity, and alternative YAP activation pathways. For example, the MST1/2 substrate, MOB1, was previously utilized as a target for a high-throughput screen of compounds with MST1/2 inhibitory effects. This screen identified a compound XMU-MP-1, which like mCLC846, demonstrated selective MST1/2 inhibition that led to up-regulation of YAP signaling and improved liver regeneration following partial hepatectomy. These findings suggest that MST1/2 inhibition can limit injury response in YAP-dependent tissues (5). We extended this previous work by evaluating MST1/2 inhibition using our orally bioavailable small molecule in murine partial hepatectomy models, including MASH models, as this represents the most severely affected population. The FFC diet utilized in our studies has been shown to recapitulate the histologic findings and metabolic changes associated with MASH (23). Importantly, we demonstrated that mice treated with mCLC846 had markedly improved survival following a 70% hepatectomy, suggesting that MST1/2 inhibition may be beneficial as a treatment to improve liver regeneration and prevent PHLF in humans, even in those with MASLD or MASH. PHLF is a complex disease and multifactorial disease process. The exact mechanism for mCLC846-induced survival is undetermined based on the data presented.

In addition to Hippo pathway targeting, alternative YAP activation pathways have been targeted for regenerative effect. We have previously demonstrated the utility of targeting the YAP-interacting phosphatase SHP2 to augment liver regeneration. Mechanistically, we had demonstrated that SHP2 negatively regulates YAP activation separately from the Hippo pathway by removing an activating phosphorylation on tyrosine 357 (4, 36, 37). Activation of YAP via this mechanism improves regeneration and limits hepatocyte injury. Like these previous studies, we found that hepatocyte YAP and the paralog TAZ were required for an augmented liver regenerative response to mCLC846, placing YAP and TAZ centrally as a rheostat for regenerative responses. Transcriptomic evaluation, however, demonstrated some notable differences in MST1/2 targeting when compared with our previous SHP2 targeting. With SHP2 targeting, we noted in vivo down-regulation of nuclear receptor 4a1 (*Nr4a1*) which functions as an apoptosis inducer and provides additional cytoprotective effects. Comparison of the transcriptomic changes in mCLC846-treated livers identified up-regulation in inflammatory signaling pathways when compared with vehicle-treated animals. Specifically, IL-17 signaling and MSP-RON signaling pathways were up-regulated in mCLC846-treated animals. IL-17 produced by $\gamma\delta$ T-cells has previously been implicated as a mitogenic signal in liver regeneration, such that exogenous IL-17 was associated with accelerated regeneration (38). Additional evidence suggests that IL-17 supports oval cell proliferation which may have implications for liver regeneration (39). These findings suggest that alteration of the inflammatory response may be a component of the beneficial effects observed with mCLC846 administration. Further delineation of these changes and their effects on underlying inflammatory states will be important, as inflammatory responses are known to be a central mediator of liver regeneration (40). Most strikingly, we noted an augmentation of the core transcriptomic changes associated with liver regeneration following partial hepatectomy. These findings again support the concept that YAP activity can behave as a rheostat regulating the regenerative potential and response following partial hepatectomy and that perioperative administration of YAP-activating molecules may have beneficial effects.

Given the potency of MST1/2 inhibition in driving hepatocyte proliferation, there are obvious concerns regarding the risk of carcinogenesis and effects on cancer. Importantly, in our studies and the previous XMU-MP-1 studies, no deleterious effects on liver function or evidence of carcinogenesis could be demonstrated even with extended dosing duration. Liver resections are performed for primary and secondary liver tumors and would expose them to mCLC846, at least temporarily. mCLC846 did increase cancer cell growth in vitro. However, washout studies demonstrated that YAP target gene levels returned to baseline within 24 h, supporting the premise that short duration, perioperative dosing would not have long-term effects on prolonged cancer cell proliferation.

Our focus has been on the effects on liver regeneration in the setting of partial hepatectomy. Small-molecule-assisted liver regeneration could also be applied to other scenarios of liver regeneration, such as liver transplantation by expanding the donor pool but would require additional investigation. Overall, the findings of this study support YAP-directed therapy as a regenerative

medicine approach and demonstrate the safety and feasibility of utilizing the MST1/2 inhibitor mCLC846 as a small molecule therapeutic in models with increased risk of PHLF.

Acknowledgments

The authors thank Jeff Janes, Mitch Hull, Hung Nguyen, and Megan Wogan (Calibr at Scripps Research) for technical assistance and Patricia Kilian, Andrew Rakeman, Peter Lomedico, and Frank Martin (all JDRF) for helpful discussions.

Supplementary Material

Supplementary material is available at *PNAS Nexus* online.

Funding

This study was supported by the Regenerative Medicine Minnesota Grant RMM092319DS009 and Optical Microscopy Core services provided through the Mayo Clinic Center for Cell Signaling in Gastroenterology (P30DK084567), and Juvenille Diabetes Research Foundation (JDRF) and the German Research Foundation (DFG).

Author Contributions

Conceptualization: R.W., E.B., M.T., W.S., and R.S. Formal analysis: C.M. Investigation: R.W., E.B., J.T., D.P., B.L., S.G., A.G., S.H.C., M.K., S.Z., S.L., S.Y., M.P., M.S., T.B., R.S., A.A., K.M., J.R., V.N.-T., S.J., M.P., N.R., and N.W.W. Writing—original draft: R.W., W.S., M.T., and R.S. Writing—review and editing: R.W., P.S., G.G., W.S., and R.S. Supervision: C.W., G.G., M.T., A.C., W.S., and R.S. Funding acquisition: K.M., G.G., W.S., and R.S.

Data Availability

Partial restrictions to the data and materials apply. All data are available upon request. Materials provided as gifts from collaborators will need to be requested through the individual donors as indicated in the manuscript. Data will be made available in a repository with the following doi:10.5281/zenodo.8415493.

References

1 Fausto N, Campbell JS, Riehle KJ. 2012. Liver regeneration. *J Hepatol*. 57(3):692–694.
2 Michalopoulos GK, Bhushan B. 2021. Liver regeneration: biological and pathological mechanisms and implications. *Nat Rev Gastroenterol Hepatol*. 18(1):40–55.
3 Russell JO, Camargo FD. 2022. Hippo signalling in the liver: role in development, regeneration and disease. *Nat Rev Gastroenterol Hepatol*. 19(5):297–312.
4 Watkins RD, *et al.* 2022. SHP2 inhibition enhances yes-associated protein-mediated liver regeneration in murine partial hepatectomy models. *JCI Insight*. 7(15):e159930.
5 Fan F, *et al.* 2016. Pharmacological targeting of kinases MST1 and MST2 augments tissue repair and regeneration. *Sci Transl Med*. 8(352):352ra108.
6 Loforese G, *et al.* 2017. Impaired liver regeneration in aged mice can be rescued by silencing Hippo core kinases MST1 and MST2. *EMBO Mol Med*. 9(1):46–60.
7 Heng BC, *et al.* 2021. An overview of signaling pathways regulating YAP/TAZ activity. *Cell Mol Life Sci*. 78(2):497–512.
8 Song H, *et al.* 2010. Mammalian Mst1 and Mst2 kinases play essential roles in organ size control and tumor suppression. *Proc Natl Acad Sci U S A*. 107(4):1431–1436.
9 Ray S, Mehta NN, Golhar A, Nundy S. 2018. Post hepatectomy liver failure—a comprehensive review of current concepts and controversies. *Ann Med Surg (Lond)*. 34:4–10.
10 Calthorpe L, *et al.* 2021. Using the comprehensive complication index to rethink the ISGLS criteria for post-hepatectomy liver failure in an international cohort of major hepatectomies. *Ann Surg*. 277:e592–e596.
11 Wakai T, *et al.* 2011. Surgical outcomes for hepatocellular carcinoma in nonalcoholic fatty liver disease. *J Gastrointest Surg*. 15(8):1450–1458.
12 Hardy T, Oakley F, Anstee QM, Day CP. 2016. Nonalcoholic fatty liver disease: pathogenesis and disease Spectrum. *Annu Rev Pathol*. 11:451–496.
13 Younossi ZM, *et al.* 2016. Global epidemiology of nonalcoholic fatty liver disease-meta-analytic assessment of prevalence, incidence, and outcomes. *Hepatology*. 64(1):73–84.
14 Vodkin I, Kuo A. 2017. Extended criteria donors in liver transplantation. *Clin Liver Dis*. 21(2):289–301.
15 Chan A, *et al.* 2021. Final efficacy results of neratinib in HER2-positive hormone receptor-positive early-stage breast cancer from the phase III ExteNET trial. *Clin Breast Cancer*. 21(1):80–91.e7.
16 Ardestani A, *et al.* 2019. Neratinib protects pancreatic beta cells in diabetes. *Nat Commun*. 10(1):5015.
17 Ardestani A, Tremblay MS, Shen W, Maedler K. 2019. Neratinib is an MST1 inhibitor and restores pancreatic beta-cells in diabetes. *Cell Death Discov*. 5:149.
18 Grubman SA, *et al.* 1994. Regulation of intracellular pH by immortalized human intrahepatic biliary epithelial cell lines. *Am J Physiol*. 266(6 Pt 1):G1060–G1070.
19 Hlady RA, *et al.* 2022. Interferon drives HCV scarring of the epigenome and creates targetable vulnerabilities following viral clearance. *Hepatology*. 75(4):983–996.
20 Meng Z, Moroishi T, Guan KL. 2016. Mechanisms of Hippo pathway regulation. *Genes Dev*. 30(1):1–17.
21 Ardestani A, *et al.* 2014. MST1 is a key regulator of beta cell apoptosis and dysfunction in diabetes. *Nat Med*. 20(4):385–397.
22 Maedler K, *et al.* 2001. Distinct effects of saturated and monounsaturated fatty acids on beta-cell turnover and function. *Diabetes*. 50(1):69–76.
23 Krishnan A, *et al.* 2017. A longitudinal study of whole body, tissue, and cellular physiology in a mouse model of fibrosing NASH with high fidelity to the human condition. *Am J Physiol Gastrointest Liver Physiol*. 312(6):G666–G680.
24 Mitchell C, Willenbring H. 2008. A reproducible and well-tolerated method for 2/3 partial hepatectomy in mice. *Nat Protoc*. 3(7):1167–1170.
25 Kiourtis C, *et al.* 2021. Specificity and off-target effects of AAV8-TBG viral vectors for the manipulation of hepatocellular gene expression in mice. *Biol Open*. 10(9):bio058678.
26 Kalari KR, *et al.* 2014. MAP-RSeq: mayo analysis pipeline for RNA sequencing. *BMC Bioinformatics*. 15:224.
27 Dobin A, *et al.* 2013. STAR: ultrafast universal RNA-Seq aligner. *Bioinformatics*. 29(1):15–21.
28 Liao Y, Smyth GK, Shi W. 2013. The Subread aligner: fast, accurate and scalable read mapping by seed-and-vote. *Nucleic Acids Res*. 41(10):e108.

29 Robinson MD, McCarthy DJ, Smyth GK. 2010. Edger: a bioconductor package for differential expression analysis of digital gene expression data. *Bioinformatics*. 26(1):139–140.
30 Ge SX, Jung D, Yao R. 2020. ShinyGO: a graphical gene-set enrichment tool for animals and plants. *Bioinformatics*. 36(8): 2628–2629.
31 Odashima M, *et al*. 2007. Inhibition of endogenous Mst1 prevents apoptosis and cardiac dysfunction without affecting cardiac hypertrophy after myocardial infarction. *Circ Res*. 100(9): 1344–1352.
32 Matsuo T, *et al*. 2003. Control mechanism of the circadian clock for timing of cell division in vivo. *Science*. 302(5643):255–259.
33 Zhao B, *et al*. 2007. Inactivation of YAP oncoprotein by the Hippo pathway is involved in cell contact inhibition and tissue growth control. *Genes Dev*. 21(21):2747–2761.
34 Mooring M, *et al*. 2020. Hepatocyte stress increases expression of yes-associated protein and transcriptional coactivator with PDZ-binding motif in hepatocytes to promote parenchymal inflammation and fibrosis. *Hepatology*. 71(5):1813–1830.
35 Caruana JA, Whalen DA Jr, Anthony WP, Sunby CR, Ciechoski MP. 1986. Paradoxical effects of glucose feeding on liver regeneration and survival after partial hepatectomy. *Endocr Res*. 12(2):147–156.
36 Buckarma EH, *et al*. 2020. The YAP-interacting phosphatase SHP2 can regulate transcriptional coactivity and modulate sensitivity to chemotherapy in cholangiocarcinoma. *Mol Cancer Res*. 18(10): 1574–1588.
37 Ege N, *et al*. 2018. Quantitative analysis reveals that actin and src-family kinases regulate nuclear YAP1 and its export. *Cell Syst*. 6(6):692–708.e13.
38 Rao R, *et al*. 2014. Interleukin 17-producing gammadeltaT cells promote hepatic regeneration in mice. *Gastroenterology*. 147(2): 473–484.e2.
39 Guillot A, *et al*. 2018. Interleukins-17 and 27 promote liver regeneration by sequentially inducing progenitor cell expansion and differentiation. *Hepatol Commun*. 2(3):329–343.
40 Campana L, Esser H, Huch M, Forbes S. 2021. Liver regeneration and inflammation: from fundamental science to clinical applications. *Nat Rev Mol Cell Biol*. 22(9):608–624.